LncRNA ENST00000581911 Regulates Extraocular Muscle Remodeling by Interacting With KHSRP in Thyroid Eye Disease

Mingsu Shi,[1–4] Rongmei Zhou,[1–4] Weiai Shen,[1–4] Yu Liang,[1–4] Yihan Zhang,[1–4] Lingyun Liu,[1–4] Runyi Shao,[5] Yanxi Fang,[1–4] Chen Zhao,[1–4] and Lianqun Wu[1–4]

[1]Eye Institute and Department of Ophthalmology, Eye and ENT Hospital, Fudan University, Shanghai, China
[2]Key Laboratory of Myopia and Related Eye Diseases, National Health Commission (NHC), Shanghai, China
[3]Key Laboratory of Myopia and Related Eye Diseases, Chinese Academy of Medical Sciences, Shanghai, China
[4]Shanghai Key Laboratory of Visual Impairment and Restoration, Shanghai, China
[5]School of Basic Medical Science, Fudan University, Shanghai, China

Correspondence: Lianqun Wu, Eye Institute and Department of Ophthalmology, Eye & ENT Hospital, Fudan University, 83 Fenyang Rd., Shanghai 200031, China; lianqun.wu@fdeent.org.
Chen Zhao, Eye Institute and Department of Ophthalmology, Eye & ENT Hospital, Fudan University, 83 Fenyang Rd., Shanghai 200031, China; dr_zhaochen@fudan.edu.cn.

Received: October 12, 2024
Accepted: February 24, 2025
Published: March 21, 2025

Citation: Shi M, Zhou R, Shen W, et al. LncRNA ENST00000581911 regulates extraocular muscle remodeling by interacting with KHSRP in thyroid eye disease. *Invest Ophthalmol Vis Sci.* 2025;66(3):46. https://doi.org/10.1167/iovs.66.3.46

Purpose. Thyroid eye disease (TED) is a visually debilitating and cosmetically disfiguring orbital disorder, characterized by the remodeling of extraocular muscles (EOMs). This study aimed to investigate the role of long non-coding RNA (lncRNA) ENST00000581911 in the EOMs of TED.

Methods. LncRNA microarray analysis was performed on EOM tissues sampled from patients with TED and patients with concomitant esotropia. LncRNA ENST00000581911 was identified and subjected to bioinformatics analysis. High-throughput RNA sequencing, CCK-8 assay, CFSE staining, and ELISA were used to investigate the regulatory function of ENST00000581911 in vitro. Furthermore, RNA pull-down, liquid chromatography-tandem mass spectrometry (LC-MS/MS), and western blot (WB) analyses were applied to identify the RNA-binding protein (RBP) interacting with ENST00000581911.

Results. A total of 1261 lncRNAs were found to be differentially expressed in the EOMs of TED, with 648 upregulated and 613 downregulated lncRNAs. Among these, the upregulated lncRNA ENST00000581911 exhibited the highest expression level, as validated by quantitative real-time PCR (qRT-PCR). Functional analysis demonstrated that ENST00000581911 might be involved in inflammatory response, regulation of muscle contraction, and amino sugar and nucleotide sugar metabolism. RNA sequencing of ENST00000581911-overexpressing and control orbital fibroblasts (OFs) showed that ENST00000581911 might play a regulatory role in DNA replication, extracellular matrix, and cell cycle. Furthermore, KHSRP was identified as the RBP of ENST00000581911. Overexpression of ENST00000581911 promoted cell proliferation and hyaluronic acid secretion in OFs, whereas silencing KHSRP attenuated these effects.

Conclusions. This study provides novel insights into the role of lncRNA ENST00000581911 in the pathogenesis of EOM remodeling in TED. ENST00000581911 may serve as a potential therapeutic target of TED.

Keywords: long non-coding RNA (lncRNA), thyroid eye disease (TED), extraocular muscle (EOM), tissue remodeling

Thyroid eye disease (TED), also known as thyroid-associated ophthalmopathy or Graves' ophthalmopathy, is a visually debilitating and cosmetically disfiguring orbital disorder.[1] Patients with TED may experience symptoms such as exophthalmos, eyelid retraction, swelling of periorbital tissues and conjunctiva, eye movement dysfunction (including strabismus and diplopia), and even visual loss. These manifestations can lead to decreased work ability, diminished quality of life, and impaired mental health.[2]

Extraocular muscles (EOMs) are frequently affected in TED, with nearly 70% of patients with Graves' disease showing EOM expansion,[1] and 17% to 50% of patients with TED developing strabismus due to severe EOM expansion.[2] EOM expansion results from tissue remodeling processes, including excessive cell proliferation, inflammation, fibrosis, and extracellular matrix secretion. Orbital fibroblasts (OFs) are key players in these pathological changes. As targets of autoimmune responses in TED, OFs are activated to synthesize hyaluronic acid (HA) and differentiate into myofibroblasts.[3,4] However, the mechanisms regulating these processes remain unclear and are subject to ongoing investigation.

Long non-coding RNAs (lncRNAs) are functional RNA molecules longer than 200 nucleotides that do not encode proteins.[5] LncRNAs have been shown to regulate gene expression at various levels, including chromosome imprint-

ing, cell-cycle control, transcription, and post-transcriptional processing.[6] They are involved in a wide range of physiological processes, such as apoptosis, proliferation, and differentiation, and are associated with individual development. In addition, dysregulation of lncRNAs plays a significant role in many human diseases, such as cancers, cardiovascular diseases, inflammatory diseases, and autoimmune diseases.[7–10] However, the biological roles and clinical significance of lncRNAs in TED remain largely unknown.

To reveal the potential role of lncRNAs in the EOMs of TED, we performed lncRNA expression profiling and compared their expression differences between EOM tissues sampled from patients with TED and patients with concomitant esotropia (CET) using microarray analysis. Among the differentially expressed lncRNAs, the upregulated lncRNA ENST00000581911 exhibited the highest expression level, as validated by quantitative real-time PCR (qRT-PCR). Functional analysis indicated that ENST00000581911 might be involved in EOM remodeling in TED. Furthermore, high-throughput RNA sequencing, along with the subsequent cell counting kit-8 (CCK-8), carboxyfluorescein diacetate succinimidyl ester (CFSE) staining, and enzyme-linked immunosorbent assay (ELISA), demonstrated that ENST00000581911 promoted cell proliferation and HA secretion of OFs in vitro. Subsequent RNA pull-down assay, liquid chromatography-tandem mass spectrometry (LC-MS/MS) and western blot (WB) analysis identified KH-type splicing regulatory protein (KHSRP) as the binding protein of ENST00000581911. Further investigations revealed that ENST00000581911 interacted with KHSRP to regulate OF function. This study provides novel insights into the role of lncRNAs, particularly ENST00000581911, in the pathogenesis of EOM remodeling in TED.

Methods

Sample Collection and Ethics Statement

EOM samples were collected from the surgical wastes of eight patients with TED and eight patients with CET who underwent strabismus surgery. All EOMs were lateral rectus muscles. Samples no. 1 to no. 5 from each group were used for RNA extraction, and samples no. 6 to no. 8 were used for the primary culture of OFs. These EOM samples were entirely distinct and did not overlap with those used in the previously published work.[11,12]

TED was diagnosed according to the Bartley criteria in 1995.[13] Patients were assessed for disease activity using the clinical activity score (CAS) system, whereas the severity of the condition was determined based on the guidelines provided by the European Group on Graves' Orbitopathy.[14–16] All patients with TED included in our study were classified as moderate-to-severe with a CAS of less than 3. Lateral rectus resection were performed due to residual esotropia after maximal bilateral medial rectus recession in those patients, as also suggested by the American Adult Strabismus Preferred Practice Pattern.[17] Steroid or immunosuppressive treatment was discontinued for at least 3 months before surgery. Patients with TED with a history of radioactive iodine therapy or thyroidectomy and other systemic/ocular inflammatory or autoimmune diseases were excluded from the study. All patients with CET exhibited normal versions and ductions, and showed no clinical signs of abnormal contractility, as confirmed by the forced duction test. Besides, patients with CET had no history of local or systemic autoimmune and inflammatory diseases, strabismus or orbital surgeries, thyroid disease or orbital diseases. The baseline demographic and clinical characteristics of patients with TED and patients with CET are listed in Supplementary Table S1.

Our study was approved by the Ethics Committee of the Eye & ENT Hospital, Fudan University (2020070 and 2022144). All above procedures were handled in accordance with the Helsinki Declaration. Written informed consent for sample collection was taken from every enrolled participant before the study began. The human tissue experiments complied with the guidelines of the ARVO Best Practices for Using Human Eye Tissue in Research (Nov2021).

RNA Extraction

Total RNA was isolated using the TRIzol reagent (Invitrogen, Carlsbad, CA, USA) according to the manufacturer's instructions. Nuclear and cytoplasmic RNA were extracted using a Cytoplasmic and Nuclear RNA Purification Kit (Norgen Biotek, Thorold, ON, Canada) following the manufacturer's instructions. RNA quantity and quality were measured by a NanoDrop 2000 spectrophotometer (Thermo Fisher Scientific, Waltham, MA, USA). Samples with an OD260/280 ratio between 1.8 and 2.1 were considered acceptable. RNA integrity was evaluated using an Agilent 2100 bioanalyzer (Agilent Technologies, Palo Alto, CA, USA), with samples having an RNA integrity number (RIN) > 7 selected for subsequent treatments.

LncRNA and Gene Microarray Analysis

LncRNA and gene microarray analysis, including labeling, hybridization, and scanning, was performed by Shanghai Kangchen Biotech (Shanghai, SH, China) using the Arraystar Human LncRNA Microarray V4.0 (Arraystar, Rockville, MD, USA). In brief, RNA samples were labeled using an Arraystar RNA Flash Labeling Kit (Arraystar) in accordance with the manufacturer's protocol. MRNA was purified from total RNA after rRNA removal using the mRNA-ONLY Eukaryotic mRNA Isolation Kit (Epicentre, Madison, WI, USA). Each sample was then amplified and transcribed into fluorescent cRNA across the entire length of the transcripts without 3′ bias utilizing a random priming method. The labeled cRNAs were purified using the RNeasy Mini Kit (Qiagen, Hilden, NRW, Germany), and their concentration and specific activity were measured by NanoDrop 2000 (Thermo Fisher Scientific).

Subsequently, the labeled cRNAs were hybridized to the Agilent SureHyb microarray (Agilent Technologies) to allow for specific binding of labeled RNA to complementary DNA probes on the array. After hybridization, the microarrays were washed to remove any non-specifically bound RNA. The arrays were then fixed and scanned using the Agilent DNA Microarray Scanner (Agilent Technologies) to capture the fluorescent signals. Signal intensities were extracted using the Agilent Feature Extraction version 11.0.1.1 software (Agilent Technologies). To ensure comparability of data across different samples, the raw signal intensities were normalized using the Agilent GeneSpring GX version 12.1 software (Agilent Technologies). Following quantile normalization, lncRNAs and mRNAs that had flags in "Present" or "Marginal" status ("All Targets Value") in at least 5 out of 10 samples were selected for further analysis.

Investigative Ophthalmology & Visual Science

The original data of microarray analysis have been deposited in NCBI's Gene Expression Omnibus (GEO)[18] and are accessible through GEO Series accession number GSE278934 (https://www.ncbi.nlm.nih.gov/geo/query/acc.cgi?acc=GSE278934).

Functional Analysis of Differentially Expressed LncRNAs

The Agilent GeneSpring GX version 12.1 software (Agilent Technologies) was used for statistical analysis to determine significant differences in expression levels between TED and control groups. Differentially expressed lncRNAs and genes were screened using the cutoff criteria of P value < 0.05 and $|\log2$ Fold change (FC)$| > 1$.

To explore the potential regulatory roles of the differentially expressed lncRNAs, we performed subtype analysis including natural antisense lncRNAs and long intergenic non-coding RNAs (lincRNAs). Gene Ontology (GO; http://geneontology.org/)[19] and Kyoto Encyclopedia of Genes and Genomes (KEGG; https://www.kegg.jp/)[20] analyses were conducted to show the functional enrichment of the differentially expressed lncRNAs using R based on the hypergeometric distribution, with a cutoff criterion of P value < 0.05. R (version 3.2.0) was used to draw the column diagram and bubble diagram of the significant enrichment term.

Additionally, we conducted joint analysis of lncRNAs and their corresponding genes to identify potential interactions and regulatory networks. Pearson's correlation test was used to assess the correlation between differentially expressed lncRNAs and genes. LncRNA-gene pairs with a P value $<$ 0.05 and Pearson's correlation coefficient (PCC) > 0.8 were screened and visualized using a circos plot[21] and a co-expression network.

qRT-PCR Validation

Total RNA was reversely transcribed using a HiScript IV All-in-One Ultra RT SuperMix for qPCR (Vazyme, Nanjing, JS, China) and amplified by qRT-PCR with a Taq Pro Universal SYBR qPCR Master Mix (Vazyme) on a LightCycler 480 II Real-time PCR instrument (Roche, Basel, Switzerland). The housekeeping gene β-actin or glyceraldehyde 3-phosphate dehydrogenase (GAPDH) was applied as an internal control. The $2^{-\Delta\Delta Ct}$ method was adopted to quantify the relative quantification of gene expression levels.[22] All primers used for qRT-PCR are shown in the Table.

Primary Culture and Transfection of OFs

Primary OFs were cultured as described previously.[23] Briefly, tissue explants were minced and plated in 10 cm culture dishes with high-glucose Dulbecco's modified Eagle's medium (DMEM; Gibco, Gaithersburg, MD, USA) containing 20% fetal bovine serum (FBS; Gibco) and 1% penicillin/streptomycin (Gibco). The cultures were incubated at 37°C in a humidified atmosphere with 5% CO_2. Once fibroblasts had grown from the explants, they were passaged after detachment with trypsin/ethylenediaminetetraacetic acid (EDTA; Gibco), and the cultures were maintained in high-glucose DMEM containing 10% FBS and 1% penicillin/streptomycin using conventional cell culture techniques. All studies utilized cells between the third and tenth passages, and cells from the same passage were used within each individual experiment to ensure consistency.

Table. Primer Sequences for qRT-PCR in This Study

Genes	Sequences (5′–3′)
β-actin	Forward: GTGGCCGAGGACTTTGATTG
	Reverse: CCTGTAACAACGCATCTCATATT
ENST00000454470	Forward: CTACAGGCACTTCAGGTCAAA
	Reverse: TAAATGCTGGGCTGTTTCG
ENST00000529081	Forward: CCTTCCATTGGTTTGCAGAC
	Reverse: ATCCCATCTGTTTGACTGAGGT
NR_038849	Forward: GTACTGGAGGAGCCATTAACAA
	Reverse: CTGAGAAACCCAGTTCCTTAGA
ENST00000424343	Forward: CTCAGCAAAGCAAGAGCCA
	Reverse: ATGAGCATCGCGGTGACTA
ENST00000422831	Forward: CATCTGTCCTGATTGCCCTAC
	Reverse: GGGTTACAGAAACTCCTAAGGC
T371450	Forward: ACCACCAGACTTCCCCATT
	Reverse: GCCTAAAGGGTCTTGTTGGA
T127417	Forward: TACACCCAAGGGAACTGAAA
	Reverse: ACGATTGGTTAATCCACTCATC
T277939	Forward: GTGTTGACATTCTGCTTGGTTG
	Reverse: ACCTTGATTCCGCTCAGTCG
ENST00000581911	Forward: AGGAATGAGGGGTAAAAGATGC
	Reverse: TTGGGGACAGATAGGGTTGC
NR_110771	Forward: CCATAGCAGCCACAAAAGG
	Reverse: TGGGGTTGACAGACAGGTT
U2	Forward: CATCGCTTCTCGGCCTTTTG
	Reverse: TGGAGGTACTGCAATACCAGG
U6	Forward: CTCGCTTCGGCAGCACA
	Reverse: AACGCTTCACGAATTTGCGT
GAPDH	Forward: AGAAGGCTGGGGCTCATTTG
	Reverse: AGGGGCCATCCACAGTCTTC

For the transfection experiments, OFs were all derived from the EOMs of control patients. OFs were seeded into 24-well plates at a density of 1×10^4 cells per well. The following day, OFs were transfected with an adenovirus (ThinkGene, Shanghai, SH, China) to overexpress ENST00000581911 (MOI = 2000) or with 50 nM siRNA (Genomeditech, Shanghai, SH, China) using Lipofectamine RNAiMAX Reagent (Invitrogen) to silence KHSRP. Cells transfected with empty adenovirus vectors (ThinkGene) or scrambled siRNAs (Genomeditech) served as negative controls. SiRNA sequences used for KHSRP were 5′-GTTGGAAGATGGAGATCAA-3′ for si1, 5′-CCCGAGAAGATTGCTCATATA-3′ for si2, and 5′-GCCTACTACTCACACTACT-3′ for si3.

High-Throughput RNA Sequencing and Differentially Expressed Gene Analysis

High-throughput RNA sequencing and analysis were conducted by OE Biotech (Shanghai, SH, China). RNA libraries were constructed using TruSeq Stranded mRNA LT Sample Prep Kit (Illumina, San Diego, CA, USA) according to the manufacturer's instructions. Then, the libraries were sequenced on an Illumina HiSeq X Ten platform (Illumina) and 150 bp paired-end reads were generated. About 50 M raw reads for each sample were generated. Raw data of fastq format were firstly processed using fastp[24] and the low-quality reads were removed to obtain the clean reads. Then, about 45 M clean reads for each sample were retained for subsequent analysis. The clean reads were mapped to the human genome (GRCh38) using HISAT2.[25] FPKM[26] of each

Investigative Ophthalmology & Visual Science

gene was calculated and the read counts of each gene were obtained by HTSeq-count.[27] Principal component analysis (PCA) was performed using R (version 3.2.0) to evaluate the biological duplication of the samples.

Differential expression analysis was performed using the DESeq2.[28] *Q*-value < 0.05 and |log2 FC| > 1 was set as the threshold for significantly differential expression. Hierarchical cluster analysis (HCA) of differentially expressed genes (DEGs) was performed to demonstrate the expression pattern of genes in different groups and samples. GO and KEGG analyses were carried out as described before. Gene set enrichment analysis (GSEA) was performed using the GSEA software.[29] The analysis used a predefined gene set, and the genes were ranked according to the degree of differential expression in the two types of samples. Then, it was tested whether the predefined gene set was enriched at the top or bottom of the ranking list.

The original data of RNA sequencing have been deposited in NCBI's Sequence Read Archive (SRA)[30] and are accessible through SRA Series accession number PRJNA1169778 (https://www.ncbi.nlm.nih.gov/sra/PRJNA1169778).

CCK-8 Assay and CFSE Staining

Cell proliferation was assessed using CCK-8 assay and CFSE staining. OFs were seeded into 96-well plates at a density of 5000 cells per well. After cell attachment, OFs were treated with 5 ng/mL TGF-β1 (MedChemExpress, Monmouth Junction, NJ, USA) for 24 hours. Subsequently, 10 µL of CCK-8 reagent (Beyotime, Shanghai, SH, China) was added to each well, and the plate was incubated at 37°C for an additional 4 hours. The amount of formazan produced was determined by measuring absorbance at 450 nm using a Multiskan FC microplate reader (Thermo Fisher Scientific). For CFSE staining, OFs were labeled with 5 µM CFSE (Selleck, Shanghai, SH, China) in PBS for 30 minutes at room temperature in the dark, and washed with PBS 3 times. A lower CFSE intensity indicated increased cell proliferation.

ELISA Assay

OFs were treated with 5 ng/mL TGF-β1 (MedChemExpress) for 24 hours to stimulate HA secretion. After treatment, the cell culture supernatants were collected and centrifuged at 1000 g for 20 minutes to remove impurities such as cells and debris. HA concentration in the supernatants was measured using an ELISA kit (ZCIBIO, Shanghai, SH, China) following standard procedures. The absorbance was measured at 450 nm using a Multiskan FC microplate reader (Thermo Fisher Scientific). Sample concentrations were calculated based on a standard curve generated using a four-parameter logistic (4-PL) model.

RNA Pull-Down Assay

ENST00000581911 RNA was transcribed in vitro using the RiboMAX Large Scale RNA Production System (Promega, Madison, WI, USA) and biotinylated using the RNA 3′ End Desthiobiotinylation Kit (Thermo Fisher Scientific) according to the manufacturer's instructions. Agarose gel electrophoresis was used to detect the synthesized RNA on a Mini-PROTEAN system (Bio-Rad, Hercules, CA, USA). The 293T cells (ZQXZ Biotech, Shanghai, SH, China) were lysed using IP Lysis Buffer (Thermo Fisher Scientific). RNA pull-down assays were performed using the Pierce Magnetic RNA-Protein Pull-Down Kit (Thermo Fisher Scientific). Next, the desthiobiotinylated RNA was captured with streptavidin magnetic beads and incubated with whole cell lysates at room temperature for 2 hours, followed by washing and elution of the RNA binding protein (RBP) complex. The eluted proteins were subjected to silver staining using SilverXpress Silver Staining Kit (Thermo Fisher Scientific). Specific bands were excised from the gel for LC-MS/MS, followed by Western blot (WB) analysis.

Liquid Chromatography-Tandem Mass Spectrometry

The protein strips were sequentially rinsed, decolorized, dehydrated, and freeze-dried before undergoing reduction, dilation, and enzymatic hydrolysis, followed by peptide extraction and centrifugation to collect the supernatant. Proteomic data analysis was conducted by Shanghai Luming Biotech (Shanghai, SH, China) using the nano-HPLC UltiMate 3000 RSLCnano (Thermo Fisher Scientific) for peptide separation and Q-Exactive plus MS (Thermo Fisher Scientific) for analysis. The MS/MS spectra were searched using the ProteomeDiscoverer 2.5 (Thermo Fisher Scientific) against the Uniprot Homo sapiens database (https://www.uniprot.org/proteomes/UP000005640).

WB Analysis

WB analysis was conducted according to standard protocols. In brief, SDS-PAGE loading buffer (Beyotime) was added to the proteins and boiled at 95°C for 10 minutes. Then, the proteins were separated by electrophoresis on BeyoGel Elite Precast PAGE Gels (Bis-Tris, 4-20%, 15 wells; Beyotime), and then transferred to 0.45 µm polyvinylidene difluoride (PVDF) membranes (Merck, Darmstadt, HE, Germany) on a Mini-PROTEAN system (Bio-Rad). SDS-PAGE Electrophoresis buffer and transfer buffer were purchased from Beyotime. WB analysis was determined using primary antibody against KHSRP (1:2,000; Abcam, Cambridge, UK). Detection was performed using an HRP-conjugated secondary antibody (1:50,000; Abcam) and developed with Super-Signal chemiluminescent substrate (Pierce Biotech, Rockford, IL, USA) on a ChemiDoc MP imaging system (Bio-Rad).

Statistical Analysis

Statistical analysis was conducted using Prism 8 (GraphPad, Boston, MA, USA). Data are presented as the mean ± standard error. For normally distributed data, differences between or among groups were compared using two-tailed unpaired Student's *t*-test or 1-way ANOVA. For non-normally distributed data, a non-parametric test (Wilcoxon rank-sum test) was used. A P value < 0.05 was considered statistically significant. The levels of significance are indicated as follows: no significance (ns), $^{*}P < 0.05$, $^{**}P < 0.01$, and $^{***}P < 0.001$. All experiments were validated using at least three replicates.

Results

Identification of Differentially Expressed LncRNAs in the EOMs of TED

Microarray analysis was used to detect the differences of lncRNA expression profiles between the TED and the

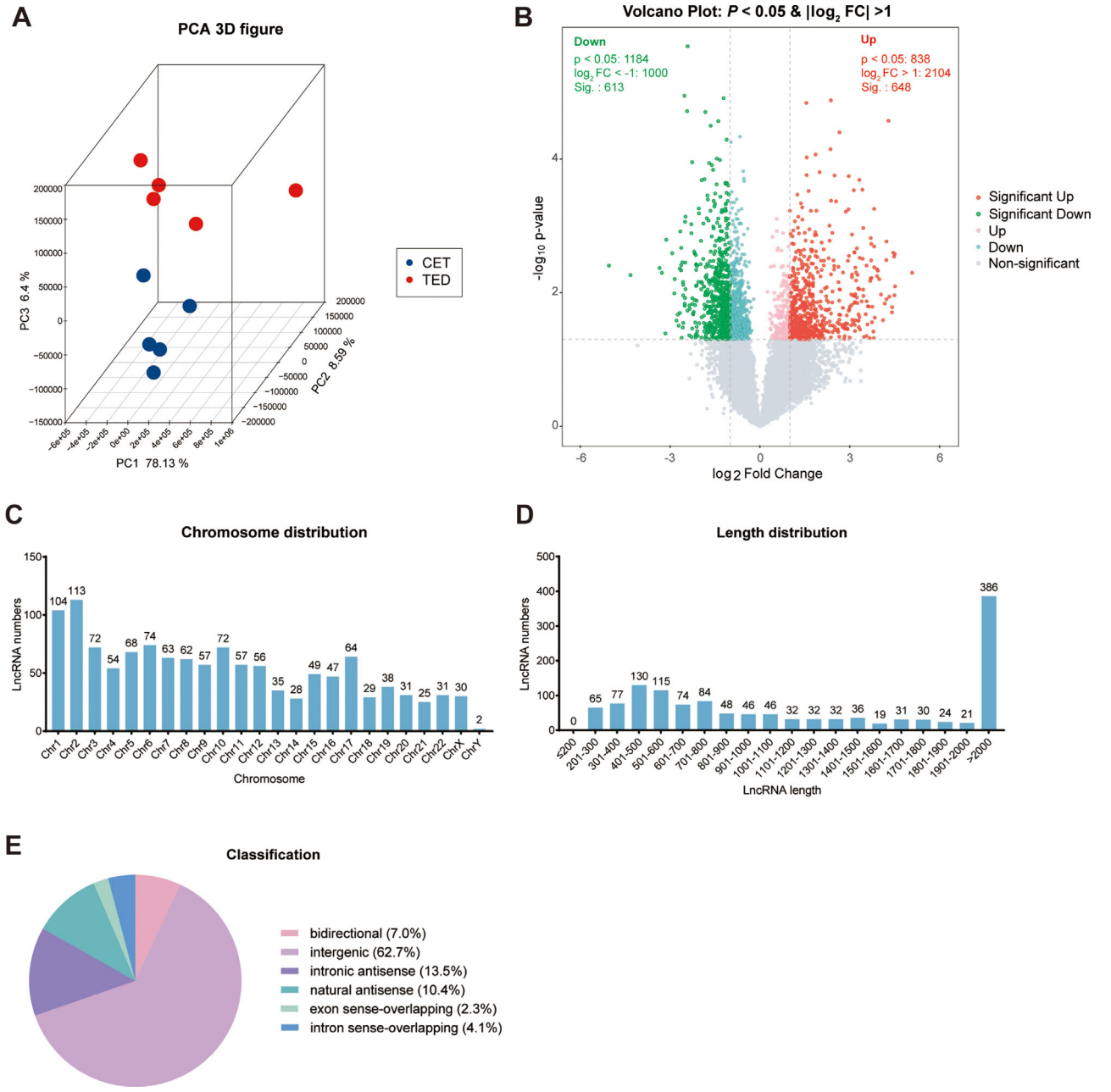

Figure 1. Long non-coding RNA (lncRNA) microarray analysis of extraocular muscles (EOMs) in thyroid eye disease (TED). (**A**) Principal component analysis (PCA) analysis showing correlations among samples. The *red dots* indicate the TED samples, and the *blue dots* indicate the constant esotropia (CET) samples. (**B**) Volcano plot depicting the screening of differentially expressed lncRNAs. The *red dots* indicate upregulation, and the *green dots* indicate downregulation. (**C**) Chromosome distribution of the differentially expressed lncRNAs. (**D**) Length distribution of the differentially expressed lncRNAs. (**E**) Classification of the differentially expressed lncRNAs based on their positional relationship with coding genes.

control groups. PCA analysis showed significant difference of lncRNA expression profiles between the TED and the control groups (Fig. 1A). Volcano plot displayed the screening of differentially expressed lncRNAs with a threshold of $P < 0.05$ and $|\log2\ FC| > 1$ (Fig. 1B). Among the 14,431 lncRNAs detected, a total of 1261 differentially expressed lncRNAs were screened out, including 648 upregulated lncRNAs and 613 downregulated lncRNAs.

Further annotation showed that these differentially expressed lncRNAs were mainly distributed on Chr2, with a length of more than 2000 nt (Figs. 1C, 1D). According to their positional relationship with coding genes, these differentially expressed lncRNAs were classified into six categories: bidirectional, intergenic, intronic antisense, natural antisense, exon sense-overlapping, and intron sense-overlapping. Among these, intergenic lncRNAs accounted for the largest proportion (Fig. 1E).

Identification of LncRNA ENST00000581911

Circos plot showed the chromosomal distribution of lncRNA-gene interaction pairs (Fig. 2A). Besides, the top

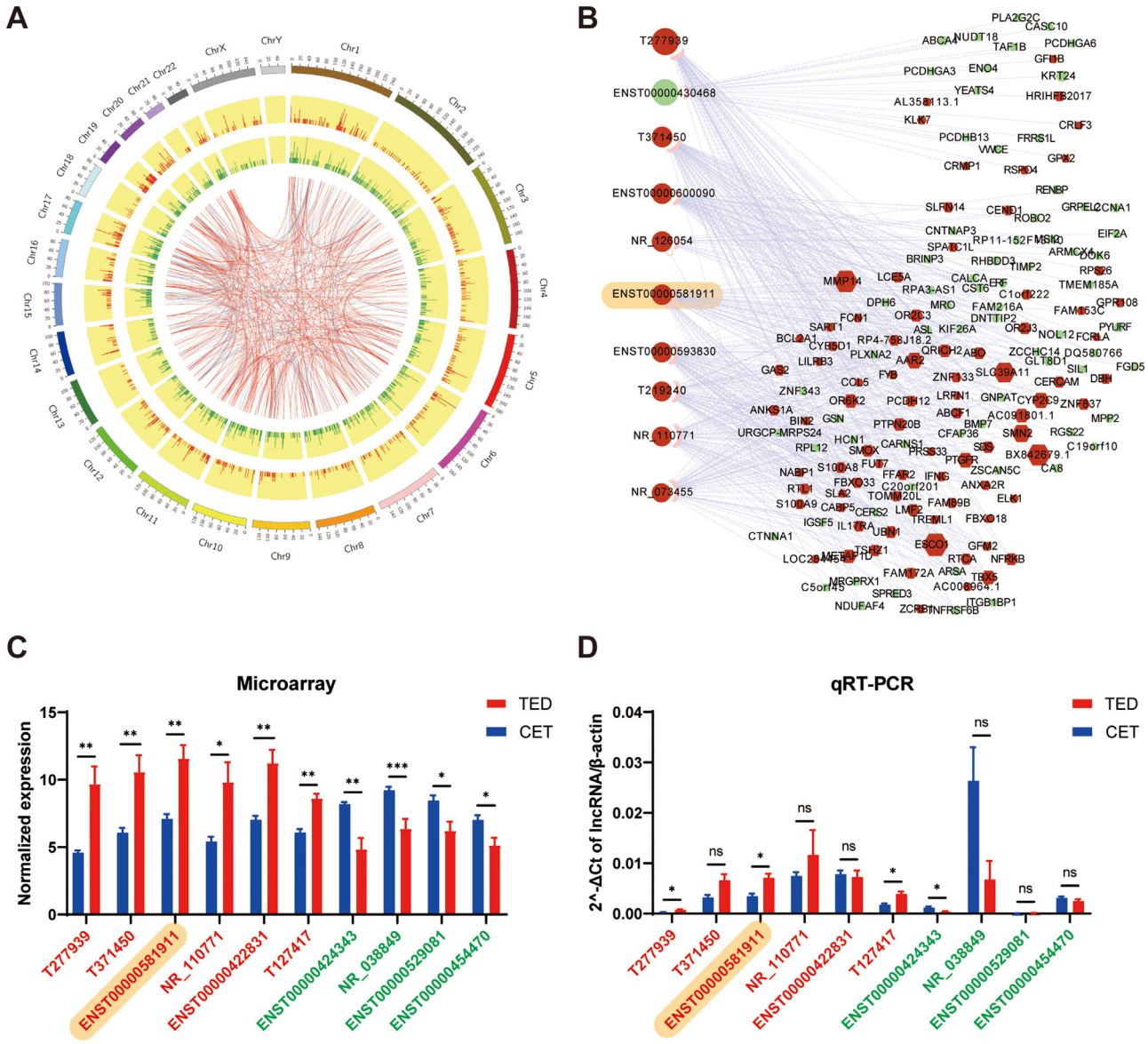

Figure 2. Bioinformatics analysis and qRT-PCR validation of the differentially expressed lncRNAs. (**A**) Circos plot showing interactions between differentially expressed lncRNAs and genes on chromosomes. In the *yellow rings*, the *red lines* represent upregulated lncRNAs, and the *green lines* represent downregulated lncRNAs. In the most *inner ring*, the *red lines* indicate positive co-expression, and the *blue lines* indicate negative co-expression. (**B**) Co-expression network between top 10 differentially expressed lncRNAs and their corresponding genes. The *red dots* indicate upregulation, and the *green dots* indicate downregulation. (**C**) Normalized expression levels of top 10 differentially expressed lncRNAs based on microarray data. (**D**) Relative expression levels of the top 10 differentially expressed lncRNAs to β-actin based on qRT-PCR. For **C** and **D**, the *red fonts* indicate upregulation, and the *green fonts* indicate downregulation. ENST00000581911 was *highlighted in yellow*. ns, no significance; *$P < 0.05$; **$P < 0.01$; and ***$P < 0.001$.

500 interaction pairs between the top 10 differentially expressed lncRNAs (T277939, ENST00000430468, T371450, ENST00000600090, NR_126054, ENST00000581911, ENST00000593830, T219240, NR_110771, and NR_073455) and 152 corresponding genes were used to construct the co-expression network (Fig. 2B). Among these, ENST00000581911 was significantly correlated with 66 genes, such as solute carrier family 39 member 11 (SLC39A11; PCC = 0.99, P = 1.8E-08) and matrix metallopeptidase 14 (MMP14; PCC = 0.98, P = 3.1E-07). To validate the accuracy and reliability of the microarray data, 10 lncRNAs (6 upregulated and 4 downregulated) from the top 20 differentially expressed lncRNAs were randomly selected for qRT-PCR detection. The expression trends of upregulated lncRNAs (T277939, ENST00000581911, and T127417) and downregulated lncRNA ENST00000424343 were consistent with the sequencing data (Figs. 2C, 2D). Notably, lncRNA ENST00000581911 demonstrated the highest expression level, making it the focus of our further analysis.

ENST00000581911 was Involved in EOM Remodeling of TED

According to the Ensembl Database, ENST00000581911 is an intergenic lncRNA located on the reverse strand

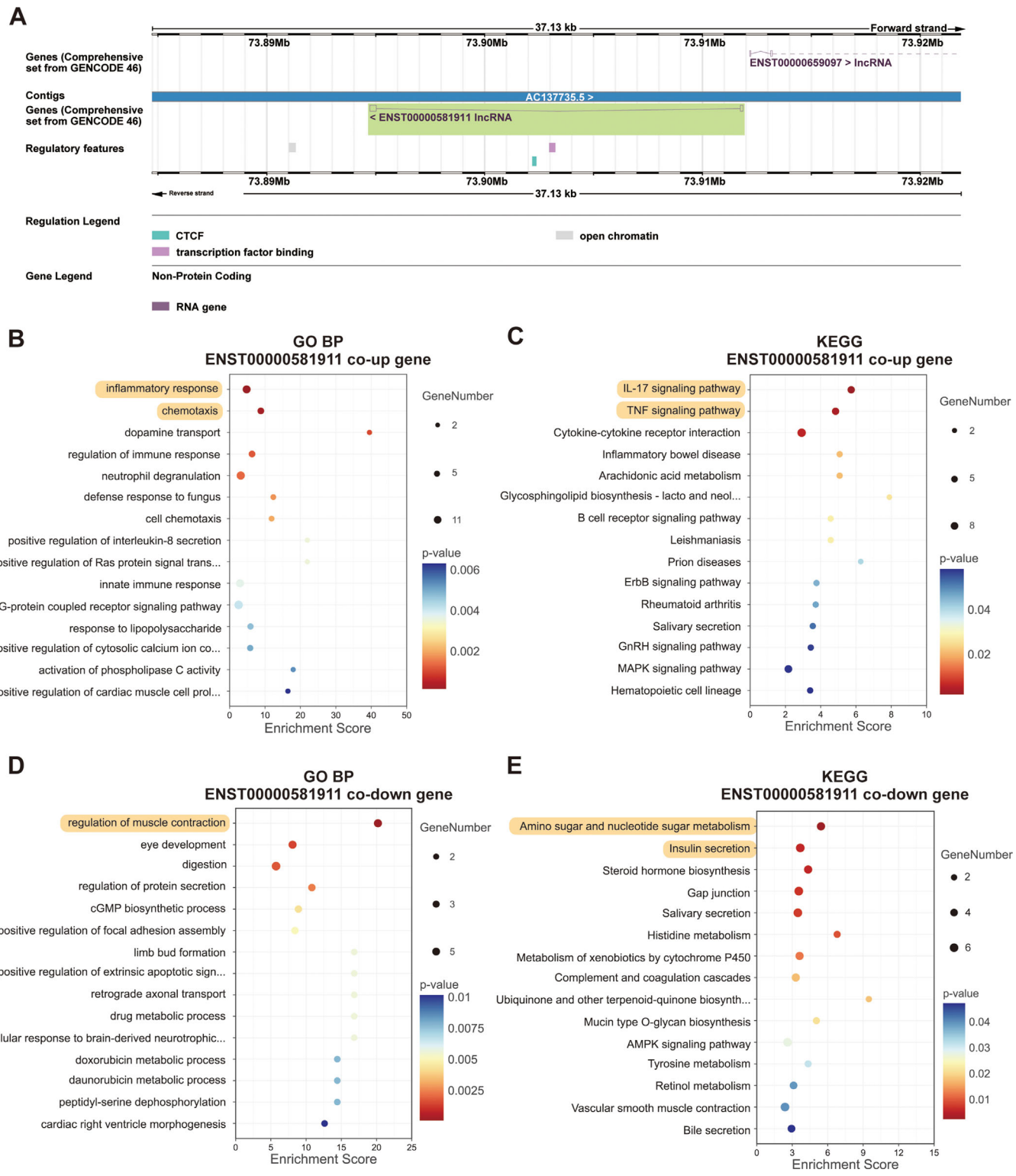

Figure 3. Functional analysis of lncRNA ENST00000581911. (**A**) Localization of the coding gene of ENST00000581911 on the genome. (**B**) Gene ontology (GO) analysis of the upregulated co-expressed genes of ENST00000581911 in the biological process (BP) category. (**C**) Kyoto Encyclopedia of Genes and Genomes (KEGG) analysis of the upregulated co-expressed genes of ENST00000581911. (**D**) GO analysis of the downregulated co-expressed genes of ENST00000581911 in the BP category. (**E**) KEGG analysis of the downregulated co-expressed genes of ENST00000581911. The top enriched terms and pathways were *highlighted in yellow*.

of Chromosome 17 (73,894,749 to 73,911,878), with a length of 419 nt (https://asia.ensembl.org/Homo_sapiens/Gene/Summary?db=core;g=ENSG00000266765;r=17:73894749-73911878;t=ENST00000581911; Fig. 3A). To explore the potential function of ENST00000581911 in vivo, we analyzed the co-expressed genes of ENST00000581911. The upregulated co-expressed genes were enriched in inflammatory response (GO:0006954, P = 1.1E-04, such

Investigative Ophthalmology & Visual Science

as PROK2 and XCR1) and chemotaxis (GO:0006935, P = 2.5E-04, such as PROK2 and RNASE2) in the biological process (BP) category according to GO analysis (Fig. 3B). Besides, KEGG analysis revealed enrichment in the IL-17 signaling pathway (hsa04657, P = 1.7E-03, such as S100A9 and S100A8) and TNF signaling pathway (hsa04668, P = 3.6E-03, such as IL18R1 and MMP14; Fig. 3C).

Conversely, the downregulated co-expressed genes were enriched in regulation of muscle contraction (GO:0006937, P = 2.9E-05, such as TNNC1 and PPP1R12B) according to GO analysis (Fig. 3D), and amino sugar and nucleotide sugar metabolism (hsa00520, P = 2.1E-03, such as MPI and NANP) and insulin secretion (hsa04911, P = 5.7E-03, such as KCNN2 and PCLO), according to KEGG analysis (Fig. 3E).

In addition, co-expressed genes involved in inflammatory response (such as CCL5 and CCL8) were used to construct a protein-protein interaction network, whereas neighboring genes of ENST00000581911 (such as CCL5 and CCL8) were used to construct a cis-regulation network (Supplementary Fig. S1). In summary, our functional analysis showed that ENST00000581911 was involved in inflammation, muscle contraction, and extracellular matrix, suggesting it might play a regulatory role in EOM remodeling in TED.

ENST00000581911 Promoted Cell Proliferation and HA Secretion in OFs

We first assessed the expression of ENST00000581911 in OFs from patients with TED and the control group using qRT-PCR. The results showed a significant upregulation of ENST00000581911 in TED OFs (Fig. 4A). Then, OFs derived from CET controls were included in further analysis. An adenovirus was constructed to overexpress ENST00000581911 in OFs, and qRT-PCR confirmed the

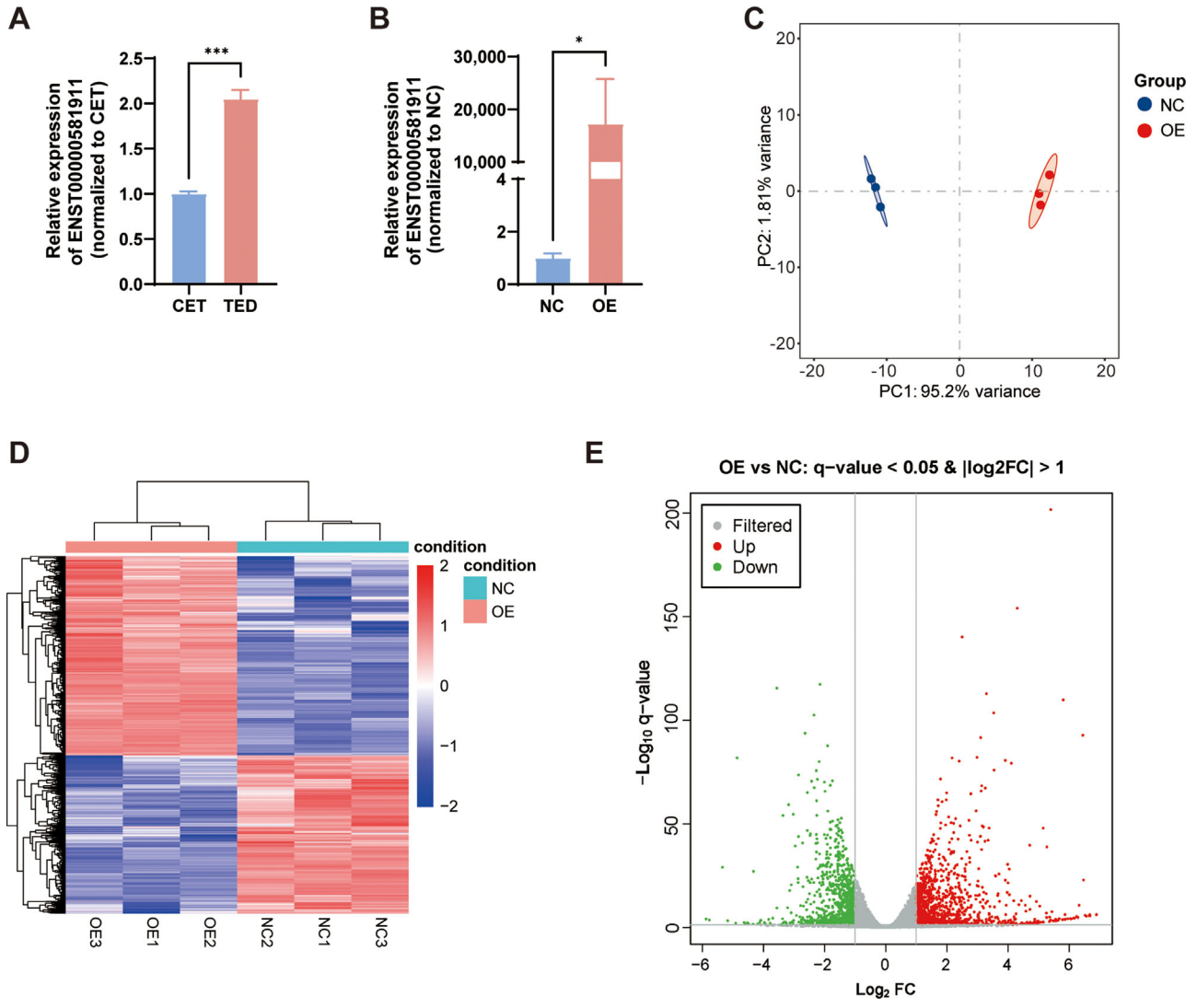

Figure 4. High-throughput RNA sequencing of ENST00000581911-overexpressed orbital fibroblasts (OFs). (**A**) Relative expression of ENST00000581911 in OFs from patients with TED and controls. (**B**) Relative expression of ENST00000581911 in ENST00000581911-overexpressed and control OFs. (**C**) PCA analysis showing correlations among samples. The *red dots* indicate ENST00000581911-overexpressed OFs, and the *blue dots* indicate negative controls. (**D**) Heatmap showing gene expression patterns of ENST00000581911-overexpressed and control OFs. The *red dots* indicate upregulated genes, and the *blue dots* indicate downregulated genes. (**E**) Volcano plot depicting the screening of differentially expressed genes (DEGs). The *red dots* indicate upregulation, and the *green dots* indicate downregulation. *P < 0.05; and ***P < 0.001.

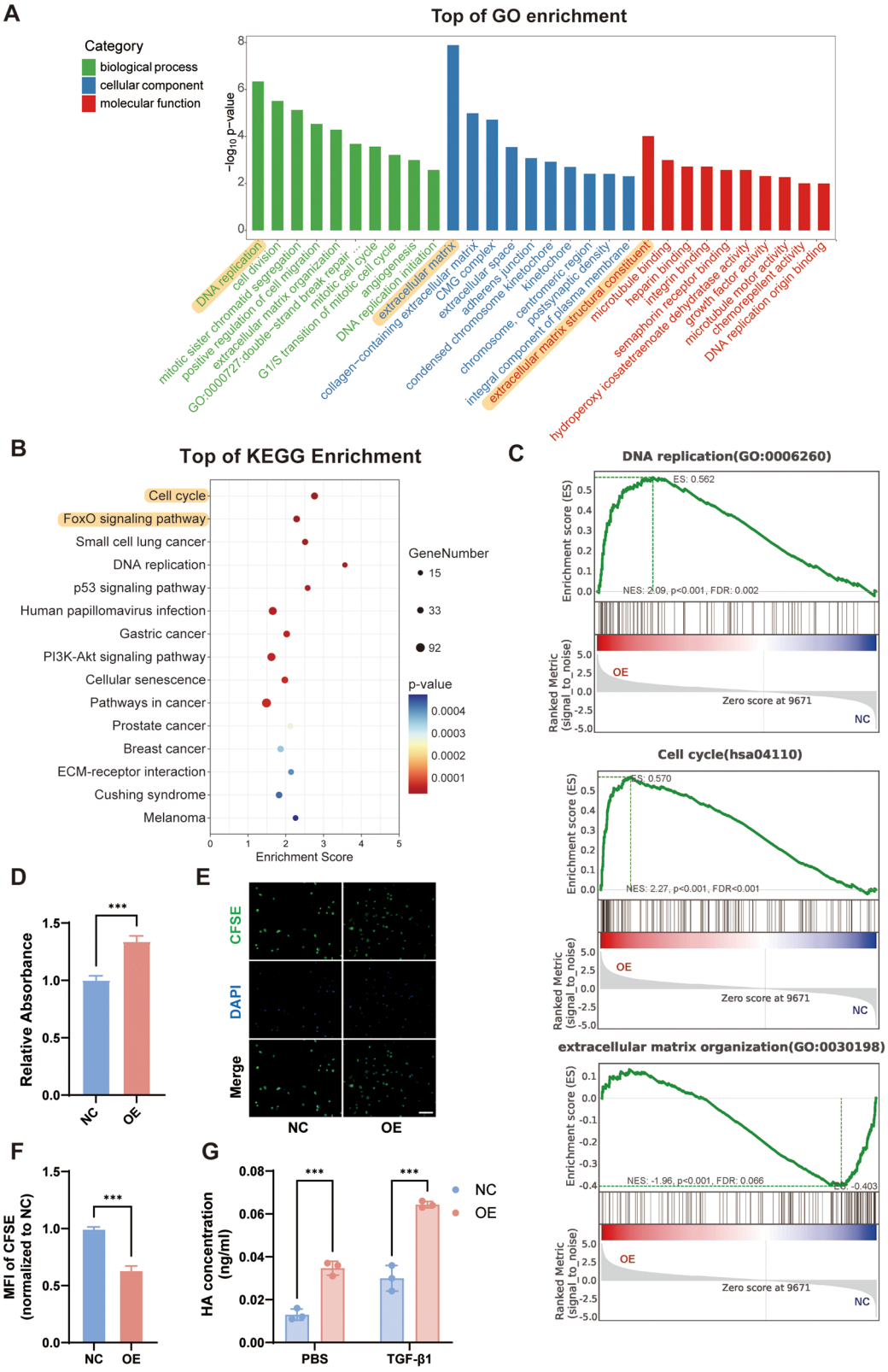

Figure 5. ENST00000581911 regulated OF function in vitro. (**A, B**) GO and KEGG analyses of the DEGs in ENST00000581911-overexpressed OFs. The top enriched terms and pathways were *highlighted in yellow*. (**C**) Gene set enrichment analysis (GSEA) analysis of gene enrichment in DNA replication, extracellular matrix, and cell cycle. (**D**) Cell counting kit-8 (CCK-8) assay of ENST00000581911-overexpressed OFs. (**E**) Carboxyfluorescein succinimidyl ester (CFSE) staining on ENST00000581911-overexpressed and control OFs. (**F**) Quantitative analysis of the normalized mean fluorescence intensity (MFI) in **E**. (**G**) Hyaluronic acid (HA) concentration in the cell culture supernatants of ENST00000581911-overexpressed OFs. ***$P < 0.001$.

Investigative Ophthalmology & Visual Science

successful overexpression following adenoviral infection (Fig. 4B).

Subsequently, we conducted high-throughput RNA sequencing on ENST00000581911-overexpressed and control OFs. PCA and HCA analyses demonstrated distinct gene expression profiles between the ENST00000581911-overexpressed and control groups (Figs. 4C, 4D). A total of 14,305 genes were identified, of which 2102 were differentially expressed (1173 upregulated and 929 downregulated; Fig. 4E).

GO analysis revealed that the DEGs were notably enriched in DNA replication (GO:0006260, $P = 1.7E-10$, such as RRM2 and FEN1) in the BP category, extracellular matrix (GO:0031012, $P = 2.4E-12$, such as ADAMTS15 and THBS2) in the cellular component category and extracellular matrix structural constituent (GO:0005201, $P = 1.6E-07$, such as THBS2 and COL8A1) in the molecular function category (Fig. 5A). KEGG analysis showed enrichment of DEGs in cell cycle (hsa04110, $P = 7.6E-10$, such as SFN and CDKN2B) and FoxO signaling pathway (hsa04068, $P = 1.5E-06$, such as CDKN2B and CCNB1; Fig. 5B). Meanwhile, GSEA analysis also highlighted gene enrichment in DNA replication, extracellular matrix, and cell cycle (Fig. 5C).

CCK-8 assay and CFSE staining results suggested that ENST00000581911 promoted the proliferation of OFs (Figs. 5D–F). Additionally, ELISA assay showed that ENST00000581911 enhanced HA secretion in OFs (Fig. 5G).

In summary, our results suggested that ENST00000581911 may play a key role in regulating gene expression involved in DNA replication, extracellular matrix, and cell cycle. This regulation appears to promote cell proliferation and HA production in OFs, which could be critical in the pathology of TED.

KHSRP Is the Binding Protein of ENST00000581911

To investigate the subcellular localization of ENST00000581911, we fractionated the nuclear and cytoplasmic components of OFs and performed qRT-PCR. The results revealed that an average of 98.3% of ENST00000581911 was localized in the nucleus (Fig. 6A). The interaction of lncRNA with RBPs, particularly those localized in the nucleus, plays a regulatory role in various cellular processes, such as gene expression, chromatin remodeling, transcriptional regulation, and RNA splicing.[31] In order to screen potential RBPs of ENST00000581911, RNA pull-down assay followed by LC-MS/MS analysis was conducted, using the antisense sequence of ENST00000581911 as a negative control (Figs. 6B, 6C). The identified proteins are listed in Supplementary Table S2.

Through an overlapping analysis of LC-MS/MS results with RBPs predicted by the RBPmap[32] and catRAPID[33] databases, as well as the upregulated genes in ENST00000581911 overexpressed OFs, KHSRP was identified as the most likely binding protein of ENST00000581911 (Fig. 6D). WB analysis further validated the binding of ENST00000581911 and KHSRP (Fig. 6E). The representative KHSRP peptides detected by LC-MS/MS are displayed in Fig. 6F, and the potential binding regions were predicted by catRAPID database (Fig. 6G). According to CELLO version 2.5,[34] KHSRP was also found to be localized in the nucleus, consistent with ENST00000581911, supporting their interaction (Fig. 6H).

ENST00000581911 Interacted With KHSRP to Regulate OF Function

To investigate the impact of KHSRP on OFs, we used siRNA to silence the expression of KHSRP. Three siRNAs targeting KHSRP were designed and transfected into 293T cells, and qRT-PCR was used to assess KHSRP expression. Among the sequences, si3-KHSRP demonstrated the highest silencing efficiency and was selected for further experiments (Fig. 7A). CCK-8, CFSE staining, and ELISA assays showed that silencing KHSRP inhibited cell proliferation and HA secretion, which reversed the functional effect of ENST00000581911 overexpression in OFs (Figs. 7B–E). In conclusion, our findings suggested that ENST00000581911 interacts with KHSRP to regulate OF function, thereby contributing to EOM remodeling in TED (Fig. 7F).

Discussion

TED is an autoimmune orbital disorder that affects orbital soft tissues, including orbital fat and EOMs. Previous studies have demonstrated the critical role of lncRNAs in the orbital fat of TED.[11,12,35] However, in TED, the pathological alterations in orbital fat and EOMs differ, and the underly mechanisms can be markedly distinct. Studies have revealed differential involvement[36] and distinct inflammatory gene expression[37] of orbital fat and EOMs in TED. Therefore, a dedicated investigation into the role of lncRNAs in the EOMs of TED is essential to advance our understanding of the disease mechanisms.

In this study, we revealed the lncRNA expression profile in the EOMs of TED using microarray analysis. Among the differentially expressed lncRNAs, a novel upregulated lncRNA, ENST00000581911 ($P = 2.9E-03$, log2 FC = 4.48), attracted our attention. Co-expression analysis identified SLC39A11 and MMP14 as the most significantly co-expressed genes with ENST00000581911. According to GO analysis, SLC39A11 was involved in plasma membrane (GO:0005886) and zinc II ion transmembrane transport (GO:0071577). MMP14, as revealed by KEGG analysis, participated in TNF signaling pathway (hsa04668), and played a vital role in extracellular matrix remodeling.[38] Additionally, CCL5 and CCL8 were identified as cis-regulated genes of ENST00000581911, which are implicated in pathological processes, such as inflammation and cancer progression.[39] These results highlighted the potential regulatory role of ENST00000581911 in EOM remodeling in TED.

To investigate the regulatory function of ENST00000581911, high-throughput RNA sequencing was performed on ENST00000581911-overexpressed OFs. The analysis revealed enrichment of DNA replication (GO:0006260) and extracellular matrix (GO:0031012) in both GO and GSEA analyses, whereas the cell cycle (hsa04110) was enriched in KEGG and GSEA analyses. Ribonucleotide reductase regulatory subunit M2 (RRM2) emerged as the most differentially expressed gene involved in DNA replication (GO:0006260). As a small subunit of ribonucleotide reductase, RRM2 facilitates the conversion of ribonucleotides to deoxyribonucleotides, ensuring a balanced dNTP pool for DNA synthesis, repair, and replication.[40,41] A disintegrin and metalloproteinase with thrombospondin motifs 15 (ADAMTS15) was the most differentially expressed gene involved in extracellular matrix (GO:0031012). The protein encoded by ADAMTS15 belongs to the proteoglycanase clade of the ADAMTS

Investigative Ophthalmology & Visual Science

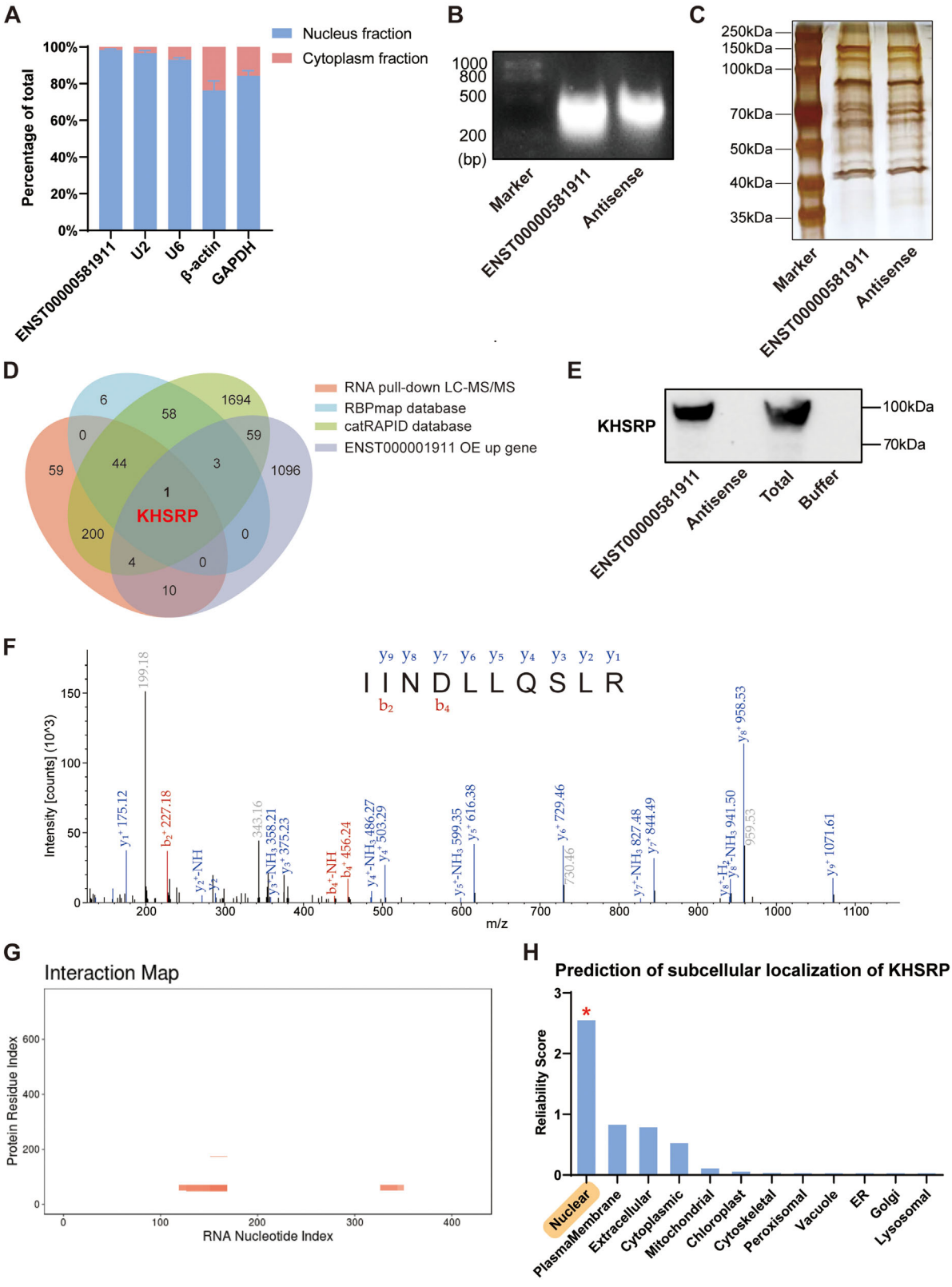

Figure 6. The binding of ENST00000581911 and KH-type splicing regulatory protein (KHSRP). (**A**) Nuclear and cytoplasmic RNA expression of ENST00000581911. (**B**) Electrophoresis of ENST00000581911 and antisense RNA. (**C**) Silver staining of the RNA binding proteins (RBPs) of ENST00000581911 and antisense RNA. (**D**) Overlapping analysis screening the most potential RBP of ENST00000581911. (**E**) Western blot (WB) analysis of KHSRP. (**F**) Representative KHSRP peptides detected by LC-MS/MS. (**G**) Potential binding regions of ENST00000581911 and KHSRP. (**H**) Subcellular localization of KHSRP.

Investigative Ophthalmology & Visual Science

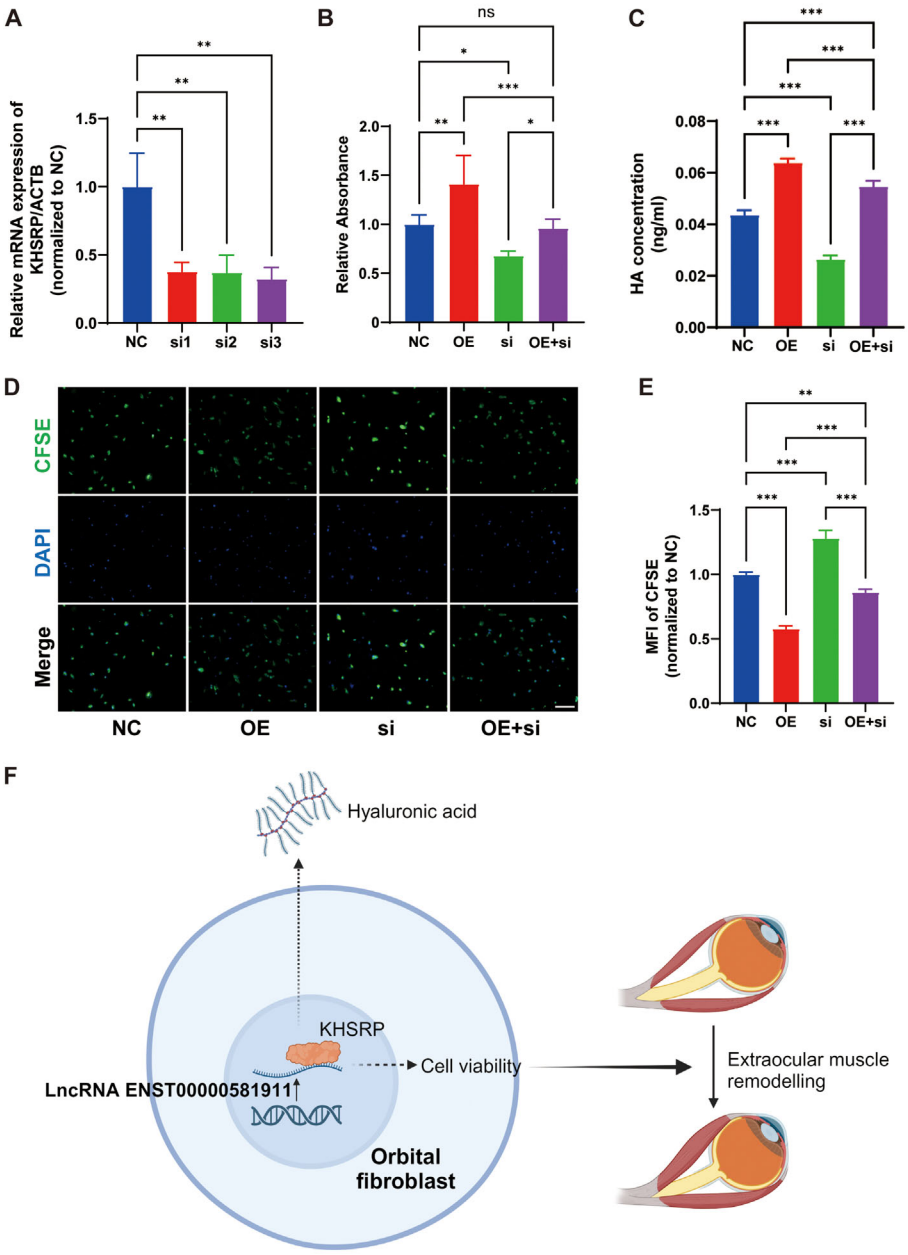

Figure 7. ENST00000581911 interacted with KHSRP to regulate OF function. (**A**) The silencing effect of three KHSRP-specific siRNAs. (**B**) CCK-8 assay of OFs. (**C**) HA concentration in the cell culture supernatants of OFs. (**D**) CFSE staining on OFs. (**E**) Quantitative analysis of the normalized MFI in **D**. (**F**) Schematic representation of the key findings in this study. NC, negative control; OE, ENST00000581911-overexpressed; si, KHSRP-silenced; OE+si, ENST00000581911-overexpressed and KHSRP-silenced. ns, no significance; $^{*}P < 0.05$; $^{**}P < 0.01$; and $^{***}P < 0.001$.

superfamily, which mediates the proteolytic degradation of extracellular matrix components, particularly targeting proteoglycans, such as aggrecan and versican.[42] SFN was the most differentially expressed gene involved in cell cycle (hsa04110). It encodes a highly conserved soluble acidic protein in the 14-3-3 family, which regulates cell cycle by interacting with p53 or AKT signaling pathways.[43,44] These results highlighted the potential roles and mechanisms of ENST00000581911 in regulating OF function.

KHSRP, known as KH-type splicing regulatory protein, is a single-stranded nucleic acid-binding protein that interacts with various RNA molecules, including mRNAs, micro RNAs, and lncRNAs, to modulate RNA stability and regulate gene expression.[45] The role of KHSRP in tissue remodeling has been demonstrated in processes such as the browning of white adipose tissue and the early phases of wound healing mediated by TGF-β.[46,47] Additionally, KHSRP's interaction with lncRNAs has been reported in several studies, such as its association with lncRNA LINC01305 in cervical cancer progression,[48] SNHG7 in endothelial-mesenchymal transition in diabetic retinopathy,[49] and AB074169 in papillary thyroid carcinoma.[50] In our study, RNA pull-down, LC-

MS/MS, and WB analyses identified KHSRP as the RBP for ENST00000581911. Further experiments confirmed that ENST00000581911 interacted with KHSRP to regulate cell proliferation and HA secretion of OF. However, the downstream mechanism by which KHSRP regulates OF function and EOM remodeling in TED requires further investigation.

In summary, our study identified lncRNA ENST00000581911 as the potential regulatory lncRNA in TED. Bioinformatics analysis suggested that ENST00000581911 plays a role of in the regulation of inflammation, muscle contraction, and extracellular matrix in the EOMs of TED. In vitro studies, including RNA sequencing, CCK-8, CFSE staining, and ELISA assays, demonstrated that ENST00000581911 regulates cell proliferation and HA secretion in OFs. Further investigations confirmed the binding and interaction of ENST00000581911 with KHSRP, revealing a potential mechanism by which ENST00000581911 modulates OF function and EOM remodeling. These findings shed new light on the molecular pathways involved in TED and suggest ENST00000581911 as a potential therapeutic target for future treatments.

However, our EOM samples were obtained from patients with moderate-to-severe TED who had a CAS < 3. This represents a limitation of our study in using CAS to identify patients, as CAS may not fully capture disease activity. Notably, a low CAS score does not necessarily indicate the absence of inflammation or the inactive stage of TED; rather, it reflects relatively stable signs and symptoms without overt inflammatory manifestations. In our study, all patients had a strabismus duration of no less than 1 year and demonstrated clinical stability for more than 6 months prior to undergoing strabismus surgery. Based on both CAS evaluation and Rundle's curve of TED progression,[51] these patients might be considered in the stable phase of the disease. However, even in this phase, disease recurrence or reactivation remains possible, underscoring the complex, dynamic interplay between pathological processes across the active and inactive stages of TED.

Our findings suggested that ENST00000581911 was associated with inflammation regulation, OF proliferation, and HA secretion, contributing to EOM remodeling. EOM remodeling is a progressively developing, dynamic pathological process that occurs throughout the course of TED, suggesting that ENST00000581911 might also play a role in early onset TED. However, further studies are essential to confirm the role of ENST00000581911 and to expand upon these findings. This could be achieved by analyzing EOM samples obtained from various stages of TED, utilizing more objective evaluations that incorporate multifactorial assessments, such as the CAS, disease duration, and magnetic resonance imaging-based parameters.

Another key limitation of our study is the use of EOMs from patients with CET as controls rather than from healthy individuals. Previous studies have indicated that patients with CET may exhibit structural and functional alterations in their EOMs,[52–54] which might not represent a truly healthy baseline. For instance, microarray analysis of strabismic EOMs has shown that genes associated with extracellular matrix structure are upregulated, and genes related to contractility are downregulated, as compared to healthy EOMs.[52] However, most of the strabismic EOMs included in this study were derived from patients with exotropia, so we do not know whether the lateral rectus muscle in patients with CET would show the same results. Patients with CET might also undergo similar changes. Thus, using patients with CET as controls may lead to misestimation of the findings regarding changes in contractility and extracellular matrix in TED EOMs. In this study, we have found that lncRNA ENST00000581911 enhances OF proliferation and HA secretion. Besides, bioinformatics analysis of microarray results has suggested that ENST00000581911 was associated with inflammation regulation in TED EOMs. However, no evidence of upregulated inflammation, OF proliferation, or HA secretion has been found in CET EOMs. Obtaining truly "healthy" human EOM tissues, however, remains a significant ethical and practical challenge. Therefore, as a compromise, we opted to use patients with CET as controls. Additionally, although OFs are the primary cellular and functional components in the EOMs of TED,[55] the observed changes in the EOMs may involve contributions from connective tissue or other components.

To address these limitations, future research should focus on using more refined control groups, such as postmortem human tissues. Besides, single-cell RNA sequencing is essential for distinguishing cell-specific changes and verifying whether the observed alterations are predominantly linked to OFs or other components. This line of investigation is currently underway. These approaches will help validate our findings and provide deeper insights into the pathology of TED.

Acknowledgments

The authors thank Qiao Zhuo and Zihan Zheng, both from the Eye Institute and Department of Ophthalmology, Eye & ENT Hospital, Fudan University, Shanghai, China, for their work in clinical sample collection.

Supported by the National Natural Science Foundation of China (82271126 to LW, 81730025 to CZ) and the Shanghai Natural Science Foundation (20ZR1409800 to LW).

Disclosure: **M. Shi**, None; **R. Zhou**, (P); **W. Shen**, None; **Y. Liang**, None; **Y. Zhang**, None; **L. Liu**, None; **R. Shao**, None; **Y. Fang**, None; **C. Zhao**, (P); **L. Wu**, (P)

References

1. Bahn RS. Graves' ophthalmopathy. *N Engl J Med*. 2010;362(8):726–738.
2. Yoo SH, Pineles SL, Goldberg RA, Velez FG. Rectus muscle resection in Graves' ophthalmopathy. *J AAPOS*. 2013;17(1):9–15.
3. Taylor PN, Zhang L, Lee RWJ, et al. New insights into the pathogenesis and nonsurgical management of Graves orbitopathy. *Nat Rev Endocrinol*. 2019;16(2):104–116.
4. Fang S, Lu Y, Huang Y, Zhou H, Fan X. Mechanisms that underly T cell immunity in Graves' orbitopathy. *Front Endocrinol (Lausanne)*. 2021;12:648732.
5. St Laurent G, Wahlestedt C, Kapranov P. The landscape of long noncoding RNA classification. *Trends Genet*. 2015;31(5):239–251.
6. Moran VA, Perera RJ, Khalil AM. Emerging functional and mechanistic paradigms of mammalian long non-coding RNAs. *Nucleic Acids Res*. 2012;40(14):6391–6400.
7. Fatima R, Akhade VS, Pal D, et al. Long noncoding RNAs in development and cancer: potential biomarkers and therapeutic targets. *Mol Cell Ther*. 2015;3:5.
8. Batista PJ, Chang HY. Long noncoding RNAs: cellular address codes in development and disease. *Cell*. 2013;152(6):1298–1307.

9. Sun M, Kraus WL. From discovery to function: the expanding roles of long noncoding RNAs in physiology and disease. *Endocr Rev*. 2015;36(1):25–64.
10. Sigdel KR, Cheng A, Wang Y, Duan L, Zhang Y. The emerging functions of long noncoding RNA in immune cells: autoimmune diseases. *J Immunol Res*. 2015;2015: 848790.
11. Wu L, Li L, Liang Y, et al. Identification of differentially expressed long non-coding RNAs and mRNAs in orbital adipose/connective tissue of thyroid-associated ophthalmopathy. *Genomics*. 2021;113(1 Pt 2):440–449.
12. Yue Z, Mou P, Chen S, Tong F, Wei R. A novel competing endogenous RNA network associated with the pathogenesis of Graves' ophthalmopathy. *Front Genet*. 2021;12:795546.
13. Bartley GB, Gorman CA. Diagnostic criteria for Graves' ophthalmopathy. *Am J Ophthalmol*. 1995;119(6):792–795.
14. Mourits MP, Prummel MF, Wiersinga WM, Koornneef L. Clinical activity score as a guide in the management of patients with Graves' ophthalmopathy. *Clin Endocrinol (Oxf)*. 1997;47(1):9–14.
15. Wu L, Zhang S, Li X, et al. Integrative transcriptomics and proteomic analysis of extraocular muscles from patients with thyroid-associated ophthalmopathy. *Exp Eye Res*. 2020;193:107962.
16. Bartalena L, Kahaly GJ, Baldeschi L, et al. The 2021 European Group on Graves' orbitopathy (EUGOGO) clinical practice guidelines for the medical management of Graves' orbitopathy. *Eur J Endocrinol*. 2021;185(4):G43–G67.
17. Dagi LR, Velez FG, Archer SM, et al. Adult strabismus preferred practice pattern. *Ophthalmology*. 2020;127(1):P182–P298.
18. Edgar R, Domrachev M, Lash AE. Gene Expression Omnibus: NCBI gene expression and hybridization array data repository. *Nucleic Acids Res*. 2002;30(1):207–210.
19. The Gene Ontology Consortium. The Gene Ontology resource: 20 years and still GOing strong. *Nucleic Acids Res*. 2019;47(D1):D330–D338.
20. Kanehisa M, Araki M, Goto S, et al. KEGG for linking genomes to life and the environment. *Nucleic Acids Res*. 2008;36(Database issue):D480–D484.
21. Krzywinski M, Schein J, Birol I, et al. Circos: an information aesthetic for comparative genomics. *Genome Res*. 2009;19(9):1639–1645.
22. Livak KJ, Schmittgen TD. Analysis of relative gene expression data using real-time quantitative PCR and the 2(-Delta Delta C(T)) Method. *Methods*. 2001;25(4):402–408.
23. Ko J, Kim YJ, Choi SH, Lee CS, Yoon JS. Yes-associated protein mediates the transition from inflammation to fibrosis in Graves' orbitopathy. *Thyroid*. 2023;33(12):1465–1475.
24. Chen S, Zhou Y, Chen Y, Gu J. fastp: an ultra-fast all-in-one FASTQ preprocessor. *Bioinformatics*. 2018;34(17):i884–i890.
25. Kim D, Langmead B, Salzberg SL. HISAT: a fast spliced aligner with low memory requirements. *Nat Methods*. 2015;12(4):357–360.
26. Roberts A, Trapnell C, Donaghey J, Rinn JL, Pachter L. Improving RNA-Seq expression estimates by correcting for fragment bias. *Genome Biol*. 2011;12(3):R22.
27. Anders S, Pyl PT, Huber W. HTSeq–a Python framework to work with high-throughput sequencing data. *Bioinformatics*. 2015;31(2):166–169.
28. Love MI, Huber W, Anders S. Moderated estimation of fold change and dispersion for RNA-seq data with DESeq2. *Genome Biol*. 2014;15(12):550.
29. Subramanian A, Tamayo P, Mootha VK, et al. Gene set enrichment analysis: a knowledge-based approach for interpreting genome-wide expression profiles. *Proc Natl Acad Sci USA*. 2005;102(43):15545–15550.
30. Katz K, Shutov O, Lapoint R, Kimelman M, Brister JR, O'Sullivan C. The Sequence Read Archive: a decade more of explosive growth. *Nucleic Acids Res*. 2022;50(D1):D387–D390.
31. Statello L, Guo CJ, Chen LL, Huarte M. Gene regulation by long non-coding RNAs and its biological functions. *Nat Rev Mol Cell Biol*. 2021;22(2):96–118. Erratum *Nat Rev Mol Cell Biol*. 2021;22(2):159.
32. Paz I, Argoetti A, Cohen N, Even N, Mandel-Gutfreund Y. RBPmap: a tool for mapping and predicting the binding sites of RNA-binding proteins considering the motif environment. *Methods Mol Biol*. 2022;2404:53–65.
33. Armaos A, Colantoni A, Proietti G, Rupert J, Tartaglia GG. catRAPID omics v2.0: going deeper and wider in the prediction of protein-RNA interactions. *Nucleic Acids Res*. 2021;49(W1):W72–W79.
34. Yu CS, Chen YC, Lu CH, Hwang JK. Prediction of protein subcellular localization. *Proteins*. 2006;64(3):643–651.
35. Zhang Z, Wu H, Gong X, et al. A comprehensive epigenetic network can influence the occurrence of thyroid-associated ophthalmopathy by affecting immune and inflammatory response. *Sci Rep*. 2024;14(1):13545.
36. Wiersinga WM, Regensburg NI, Mourits MP. Differential involvement of orbital fat and extraocular muscles in graves' ophthalmopathy. *Eur Thyroid J*. 2013;2(1):14–21.
37. Romero-Kusabara IL, Filho JV, Scalissi NM, et al. Distinct inflammatory gene expression in extraocular muscle and fat from patients with Graves' orbitopathy. *Eur J Endocrinol*. 2017;176(4):481–488.
38. Wang G, Chen S, Xie Z, et al. TGFβ attenuates cartilage extracellular matrix degradation via enhancing FBXO6-mediated MMP14 ubiquitination. *Ann Rheum Dis*. 2020;79(8):1111–1120.
39. Zeng Z, Lan T, Wei Y, Wei X. CCL5/CCR5 axis in human diseases and related treatments. *Genes Dis*. 2022;9(1):12–27.
40. Zuo Z, Zhou Z, Chang Y, et al. Ribonucleotide reductase M2 (RRM2): regulation, function and targeting strategy in human cancer. *Genes Dis*. 2024;11(1):218–233.
41. Booker S, Broderick J, Stubbe J. Ribonucleotide reductases: radical enzymes with suicidal tendencies. *Biochem Soc Trans*. 1993;21(Pt 3):727–730.
42. Dancevic CM, Fraser FW, Smith AD, Stupka N, Ward AC, McCulloch DR. Biosynthesis and expression of a disintegrin-like and metalloproteinase domain with thrombospondin-1 repeats-15: a novel versican-cleaving proteoglycanase. *J Biol Chem*. 2013;288(52):37267–37276.
43. Chauhan S, Sen S, Chauhan SS, et al. Stratifin in ocular surface squamous neoplasia and its association with p53. *Acta Ophthalmol*. 2021;99(8):e1483–e1491.
44. Li R, Yan X, Zhong W, et al. Stratifin promotes the malignant progression of HCC via binding and hyperactivating AKT signaling. *Cancer Lett*. 2024;592:216761.
45. Briata P, Bordo D, Puppo M, et al. Diverse roles of the nucleic acid-binding protein KHSRP in cell differentiation and disease. *Wiley Interdiscip Rev RNA*. 2016;7(2):227–240.
46. Chou CF, Lin YY, Wang HK, et al. KSRP ablation enhances brown fat gene program in white adipose tissue through reduced miR-150 expression. *Diabetes*. 2014;63(9):2949–2961.
47. Sundaram GM, Common JE, Gopal FE, et al. 'See-saw' expression of microRNA-198 and FSTL1 from a single transcript in wound healing. *Nature*. 2013;495(7439):103–106.
48. Huang X, Liu X, Du B, et al. LncRNA LINC01305 promotes cervical cancer progression through KHSRP and exosome-mediated transfer. *Aging (Albany NY)*. 2021;13(15):19230–19242.

Investigative Ophthalmology & Visual Science

49. Cao X, Song Y, Huang LL, Tian YJ, Wang XL, Hua LY. m6A transferase METTL3 regulates endothelial-mesenchymal transition in diabetic retinopathy via lncRNA SNHG7/KHSRP/MKL1 axis. *Genomics*. 2022;114(6):110498.
50. Gou Q, Gao L, Nie X, et al. Long noncoding RNA AB074169 inhibits cell proliferation via modulation of KHSRP-mediated CDKN1a expression in papillary thyroid carcinoma. *Cancer Res*. 2018;78(15):4163–4174.
51. Dolman PJ. Evaluating Graves' orbitopathy. *Best Pract Res Clin Endocrinol Metab*. 2012;26(3):229–248.
52. Altick AL, Feng CY, Schlauch K, Johnson LA, von Bartheld CS. Differences in gene expression between strabismic and normal human extraocular muscles. *Invest Ophthalmol Vis Sci*. 2012;53(9):5168–5177.
53. Schoeff K, Chaudhuri Z, Demer JL. Functional magnetic resonance imaging of horizontal rectus muscles in esotropia. *J AAPOS*. 2013;17(1):16–21.
54. Hao J, Wang M, Liu J, Yusufu M, Cao K, Fu J. Alteration of neurotrophic factors and innervation in extraocular muscles of individuals with concomitant esotropia. *Invest Ophthalmol Vis Sci*. 2024;65(3):1.
55. Lee ACH, Kahaly GJ. Pathophysiology of thyroid-associated orbitopathy. *Best Pract Res Clin Endocrinol Metab*. 2023;37(2):101620.

Investigative Ophthalmology & Visual Science